Detailed Characterization of An Annealed Reduced Graphene Oxide Catalyst for the Selective Peroxide Formation Activity

Tae Hoon Lee,[1,†] Sojung Park,[2,†] Tae Hwan Choi,[1,†] Liang Zhang,[3,4] Juyoung Kim,[5] Jinghua Guo,[3,6] Ho Bum Park,[1] Wooyul Kim,[2,] and Hyo Won Kim[4,7,*]*

[1]Department of Energy Engineering, Hanyang University, Seoul 04763, Korea

[2]Department of Chemical and Biological Engineering, Sookmyung Women's University, Seoul 04310, Korea

[3]Advanced Light Source, Lawrence Berkeley National Laboratory, Berkeley, California 94720, United States

[4]Institute of Functional Nano & Soft Materials (FUNSOM), Joint International Research Laboratory of Carbon-Based Functional Materials and Devices, Soochow University, 199 Ren'ai Road, Suzhou 215123, Jiangsu, China

[5]Department of Advanced Materials Engineering, Kangwon National University, Samcheok 25931, Korea

[6]Department of Chemistry and Biochemistry, University of California, Santa Cruz, California 95064, United States

[7]Department of Chemical and Biomolecular Engineering, University of California, Berkeley, California 94720, United States

ABSTRACT

Recently, electrochemical hydrogen peroxide (H_2O_2) generation from oxygen molecules has been extensively studied. Thus far, the best peroxide activity under alkaline conditions has been reported at the surface of a mild reduced graphene oxide annealed at 600 °C (mrGO-600). However, the detailed material information, such as chemical functionality and structural morphology, is unknown, which results in ambiguous debates on its catalytic active sites. To solve this problem, we intensively characterize the structure of the mrGO-600 to clarify the origin of its catalytic activity. Various characterizations, including X-ray photoelectron spectroscopy, Raman spectroscopy, infrared spectroscopy, near edge X-ray absorption fine spectroscopy, and high-resolution transmittance electron microscopy coupled with in-situ Infrared spectroelecrochemistry, reveal that the annealing process generates not only various hole edge defects that are related to the ring ether group, but also numerous point defects that result in a small-sized disconnected graphitic carbon region. These defects are believed to form a unique atomic level configuration in the mrGO-600, which enables it to facilitate high peroxide-generated activity from oxygen molecules in alkaline electrolyte.

KEYWORDS

electrocatalyst, oxygen reduction reaction, reduced graphene oxide, carbon characterization, spectroelectrochemistry

INTRODUCTION

Electrochemical hydrogen peroxide (H_2O_2), which is obtained by simultaneously reducing two electrons and protons from oxygen molecules in alkaline media, has been receiving significant attraction as a feasible route to satisfy the current demand for on-site H_2O_2 production if inexpensive electrocatalysts with high activity, selectivity, and stability are developed.[1-6] The peroxide (HO_2^- which is a deprotonated form of the H_2O_2) produced in a basic electrolyte is particularly used in the bleaching process of paper and pulp,[3, 7] which is the main target of the global hydrogen peroxide market.[6, 8] Various forms of carbon electrodes, such as glassy carbon, graphite, and meso-/micro-porous carbon, have been reported as candidates because of their cost effectiveness and relatively high peroxide selectivity.[9-11] However, they require relatively high input energy to activate the oxygen reduction reaction (ORR) due to their poor catalytic activity. Since the general catalytic efficiency strongly depends on the catalyst used, developing cost-effective carbon-based electrodes with highly selective, active, and stable catalyst is the first step toward the practical production of electrocatalytic peroxide.[1, 3]

To design a proper material, it is essential to understand correlation between catalytic properties and chemical structures (*i.e.*, chemical functionalities and structural morphologies). The objective of several studies is therefore to synthesize electrocatalysts that provide outstanding peroxide formation efficiency, and to relate catalytic activity to single active site with the aid of advanced material characterization, including *in-situ* spectroelectrochemistry and computing simulation containing density functional theory.[1, 3-6, 12] A few of the interesting materials achieved in alkaline media are oxidative nanocarbons, such as mild reduced graphene oxide (mrGO) and oxidation of carbon nanotube (O-CNT).[5, 6]

These studies found that the surface oxidation of carbon materials improved their peroxide formation activity compared with un-treated, pristine carbon materials. In particular, the O-CNT shows much higher peroxide formation activity and selectivity than the unoxidized CNT.[5] This interesting feature can be understood in terms of the density functional theory that suggests the carbon molecules near certain oxygen functional groups (such as ether and carboxylic acid) as key role players to promote ORR for enhanced peroxide formations.[5] It is important to note that oxygen incorporated into carbon materials spontaneously induce non-graphitic carbon lattices. Another representative example is the mrGO-based catalysts, which consist a small size of graphitic carbon area and ether groups on the basal plane.[6] The peroxide-generated catalytic properties of the mrGO surface exhibit close to zero overpotentials, nearly perfect selectivity, and fairly stable production when moderate potentials are applied to it.[6] Given the chemical structure of the oxidative carbons and the mrGO, the higher graphitic carbon concentration seems to create a negative impact on peroxide formation. Furthermore, 600 ^{o}C-treated mrGO (mrGO-600) surface improves the selective production of peroxide in alkaline conditions, even though there is an increase in sp^2 carbon concentration.[6] Extensive characterizations with advanced *operando* Raman spectroscopy reveal that sp^2 carbons located at grain boundary between graphitic lattice and ether or epoxy groups facilitate peroxide production efficiency, and the peroxide generation ability could be drastically improved by increasing the number of active sites.[6, 13]

These interesting outcomes are sufficient to bring the surface modification of carbon catalysts to a researcher's attention, that gives rise to a number of synthetic processes to enhance catalytic efficiency by incorporating numerous surface defects such as doping heteroatom or

creating edge on carbon electrocatalysts.[14-19] Carbon characterization thus becomes more important to identify the correlation between catalytic activity and chemical structures.[20]

Until now, certain functionality which relates with the carbon defects has been generally believed to take part in the ORR chemistry such as activity and selectivity[5, 6, 20] that is, a single functional group facilitates one reaction. For example, the sp^2 carbons adjacent to ether groups can electrocatalytically convert to hydrogen peroxide from the oxygen molecule regardless of the pH of electrolytes.[12] This hypothesis looks very reasonable and most of the research is focused on the identification of single active sites to affect the activity and to determine the reaction selectivity.

However, in nanocarbon electrocatalysts, most of the modified nanocarbons, including graphene, graphene oxide, and carbon nanotube, report different ORR selectivity.[21-24] It is interesting to know that modified nanocarbons consist of similar chemical functional groups with different concentrations regardless of ORR activity and selectivity.[21-24] These facts indicate, there are other critical factors required to govern the ORR electrochemistry, that most studies overlooked. A very recent study for the first time reported that a specific single chemical site could not determine the ORR selectivity by itself.[25] More interestingly, this study suggested that the sp^2 carbons near oxide groups could be the most potential candidates to facilitate both $2e^-$ and $4e^-$ ORR, and the ORR properties are responsible for the general chemical environment (*i.e.*, sp^2 carbon lattice size) around the active site.[25] For example, the active site along with small sp^2 graphitic region (*i.e.*, semi-conductive site) is favorable for peroxide generation (*i.e.*, $2e^-$ ORR), while the catalytic site with large sp^2 carbon area (*i.e.*, conductive site) is likely suitable for the energy generation in fuel cell applications (*i.e.*, $4e^-$ ORR).[25] Therefore, to design an active and

selective peroxide-generated carbon electrode, several grain boundaries are required between ether or epoxy groups and sp^2 carbon regions with a small area.

However, this conclusion raises a critical question about why the mrGO-600 that includes abundant sp^2 carbons shows the highest peroxide formation activity and selectivity in alkaline condition when measured by the X-ray photoelectron spectroscopy (XPS),[6] which contradicts the recent reasonable results.[25] To this end, here, we intensively characterize the detailed chemical structure of the mrGO-600 by adopting infrared (IR) spectroscopy, Raman spectroscopy, X-ray based spectroscopy, and high-resolution transmittance electron microscopy (HR-TEM). In-situ IR spectroscopy is also used to figure out peroxide formation active sites in the mrGO-600. The objective is to elucidate the reason for high peroxide formation activity on the mrGO-600 surface so that these sites could incorporate catalysts where 2 e^- ORR is required in alkaline condition.

RESULTS AND DISCUSSION

The surface activity of the mrGO-600 is located in the uppermost right region of the catalytic mass activity to peroxide generation graph (Figure S1), indicating that the best peroxide formation activity is performed by mrGO-600 in comparison with other electrocatalysts as reported in basic media.[6] The highest catalytic activity of the mrGO-600 surface can be understood in terms of its unique chemical structure consisting of several ether groups reformed next to sp^2 carbons along the edge after annealing.[6, 13] This distinct chemical conformation of the mrGO can be tuned by the annealing process at 600 ^oC under an inert condition. The heat treatment sharply increases carbon-carbon bonding from 57.9 to 90.0 at.% confirmed from the surface sensitive C1s XPS results (Figure S2), and simultaneously eliminates residual oxygen functional groups on the basal plane, which generates a number of holes spontaneously.[26] The

carbon-carbon bonding changes can be easily assumed increased sp^2 carbon ratio in the mrGO-600 surface. Furthermore, the created-hole edges are attached with the rearranged ring ethers, that dramatically improves peroxide formation activity in the mrGO-600 surface.[6, 27, 28]

These configuration changes in the surface structure (*i.e.*, the increased sp^2 carbon region as well as hole-defects on the basal plane) can also be obtained from the Raman spectroscopic results coupled with the Raman mapping images (Figure 1). In particular, the morphological difference between the mrGO and the mrGO-600 reflects the confocal Raman mapping for the D/G ratio where green and black spots indicate relatively higher and lower D/G ratio, respectively. When D and G band mapping images are individually compared (Figure S3), we assume that certain black spots might be empty space, presumably due to the hole-defects area. Thus, we have focused on green spots to minimize misinterpretation. The mrGO-600 surface exhibits stronger and brighter green spots than the mrGO surface, indicating that the mrGO-600 contains larger in-plane crystallite sizes. An additional evidence that the mrGO-600 consists higher concentration of sp^2 carbon lattices, can be obtained with different ratio values (*i.e.*, 1.16 for the mrGO and 1.25 for the mrGO-600) compared with the intensity ratio of D and G bands ($\sqrt{\frac{I_D}{I_G}}$) (Figure 1a). In general, this ratio can be used as an estimation of the sp^2 lattice area and has a linear relation with the average size of sp^2 ring cluster.[29]

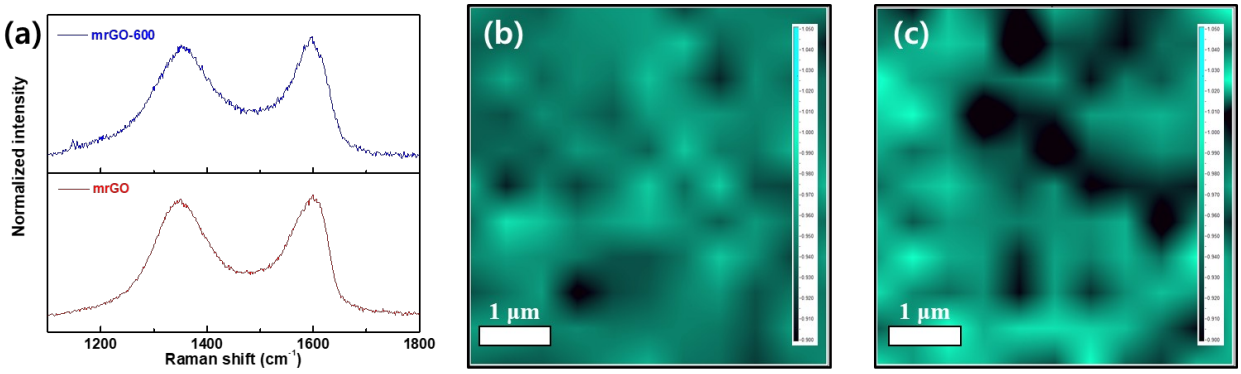

Figure 1. Raman spectra and Raman mapping. Typical Raman spectra for mrGO and mrGO-600 (a) and I_D/I_G Raman mapping of mrGO (b), and mrGO-600 (c).

This approach is well established to analyze the carbon structure. However, from the XPS data, the ratio changes appear to be much lower than expected, which means that the mrGO-600 surface is a more complex configuration. For example, if certain molecular-level defects (like Stone-Wales and vacancy defects) are located in the middle of basal plane, which is a very common situation on a GO modification process and especially thermal treatment,[30-32] these unavoidable defects have a great impact on the material properties such as mechanical strength, chemical reactivity, and thermal and electrical conductivities. Therefore, it is necessary to obtain a detailed structural and morphological information including bonding location, orientation, and size that minimizes misunderstanding on the site related to catalytic activity.

To gain further structural information, we used high resolution IR spectroscopy to clarify buried ambiguous absorption peaks (Figure 2a). It is important to note that using common IR spectroscopy it is difficult to characterize functional groups of reduced graphene oxide due to the strong tendency of destructive interference caused by the adjacent functional groups, hence the edge ether group is not observed (Figure S4). However, several interesting features can be still observed when comparing the IR spectroscopy between mrGO and mrGO-600. First, after

thermal treatment at 600 °C, a very strong peak at approximately 800 cm^{-1} along with a sharp peak at 1260 cm^{-1} shows up which corresponds to the reformation of edge ether group.[27, 28] Secondly, the mrGO-600 peaks look less complex in comparison with the mrGO, meaning that the functionality of mrGO-600 is relatively less than the mrGO. Lastly, the mrGO-600 seems to have slightly larger sp^2 carbon regions than the mrGO. This information can be obtained by roughly comparing the intensity ratio between C-OH (approximately centered at 3500 cm^{-1}) and C=C (at approximately 1675 cm^{-1}).[27, 28]

To more clarify, a near-edge X-ray absorption fine structure (NEXAFS) spectroscopy was employed, because this tool (based on the excitation of core electrons to empty or partially filled states) can afford the detection of various functional groups from discernible assigned photon energy peaks and can probe the electronic band structures of carbon related materials from C K-edge NEXAFS.[33-35] Thus, the NEXAFS seems to be more suitable for a clear understanding of chemical and structural characteristics of the mrGO-600 especially linked with the sp^2 carbon bond. This knowledge can be related to the electronic properties for a better perception on the catalytically peroxide-generated site of the mrGO-600. For example, in the C K-edge NEXAFS data, there are several characteristic peaks that describe representative carbon bonding including carbon-carbon bond assigning to the transition or excitation of C1s core-level electrons into π^* or σ^* states and carbon-oxygen bonds between the π^* and σ^* states (Figure 2b). According to previous studies, the π^* transition is generally located in the lowest energy resonance at approximately 285.0 eV, while the σ^* excitation is associated with higher energy resonance approximately centered at 292.5 eV.[33, 35] It is important to note, both energy peak positions are strongly depended on material properties. The specific oxygen functional groups

are assigned transitions from C1s core states to the localized antibonding states of each oxygen species. Functional group assignments of spectral features observed in the C K-edge are attributed to hydroxyl at ~ 286.6 eV, carbonyl at ~ 288.7 eV, carboxylic acid at ~ 289.9 eV, and epoxide (or ether) at ~ 287.7 eV, respectively.[33-35]

In particular, position of the lowest energy peak at approximately 285.0 eV, which is responsible for the transition of C1s core level into the π^* states, can be varied and its intensity can be altered depending on the degree of reduction of oxygen functional groups and status of restoration of graphitic sp^2 carbon region.[33, 35] For instance, increasing deoxygenation moves the peak position to positive, and larger sp^2 hybridized carbon makes the peak intensity sharp.[33, 35] The lowest peaks of both materials are indeed located in different peak positions centered at 284.0 eV for the mrGO and 285.5 eV for mrGO-600, indicating that the mrGO-600 contains less oxygen functional groups than the mrGO, which corresponds with IR spectroscopy data (Figure 2b). However, no strong and sharp peak intensities are observed in both the catalysts, although the shape of graph is different. On the one hand, the mrGO suddenly represents π^* resonance at 284.0 eV, which means the mrGO consists of isolated aromatic sp^2 carbon region with small size. On the other hand, the mrGO-600 gradually increases the signal before showing π^* resonance at approximately 285.5 eV, which presumes that the mrGO-600 contains high sp^2 carbon concentration consists of isolated and non-continuous aromatic sp^2 carbon regions (Figure 2b). This discontinuous sp^2 carbon region might be caused by the high temperature annealing process, because the thermal treatment might spontaneously generate a number of holes and oxygen atom inclusion defects in the middle of basal plane that disturbs the well-ordered and continuous sp^2 carbon bonds. Hence, the mrGO-600 mainly consists of several isolated aromatic sp^2 carbons with small graphitic size.

During the annealing, substantial CO_2 and CO evolutions are indeed observed and two different temperatures starting at approximately 150 °C and 500 °C are confirmed from thermos-gravimetric analysis equipped with mass spectrometry (TGA-MASS). This indicates the elimination of oxygen along with carbon from the mrGO (Figure S4). The lower decomposition temperature serves as deoxygenation on the basal plane, and the higher temperature can create several holes, which might interrupt sp^2 carbon bonding connectivity. It is a reasonable assumption because the mrGO treated at 300 °C (denotes at mrGO-300) shows the strongest and sharpest energy peak at the π^* transition among them (Figure S5), although the peak intensity is not significantly strong to compare with other sp^2 carbon dominant materials.[25]

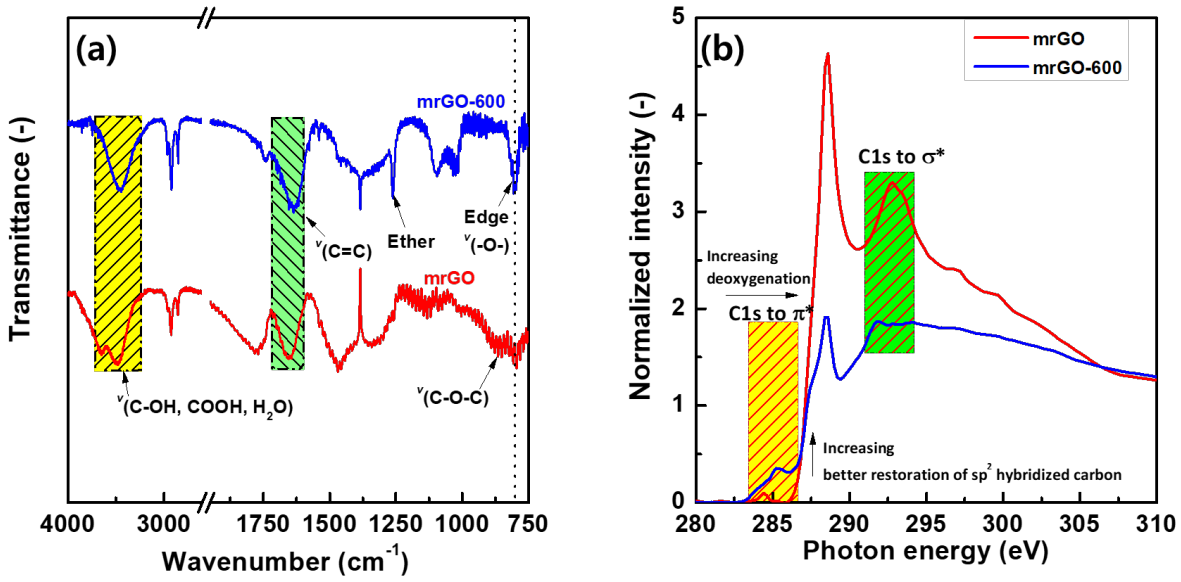

Figure 2. Spectroscopic results of mrGO and mrGO-600. IR (a) and NEXAFS (b) spectroscopy.

A representative HR-TEM image shows that the mrGO's graphitic carbons are surrounded by abundant amorphous carbons that can be expected from the characteristic results (Figure 3a). The mrGO-600 appears to be more complex surface morphology to characterize, because of the presence of numerous point defects including pinholes and mismatched six

membered rings in the middle of graphitic sp^2 carbon regions (Figure 3b). This indicates that the higher degradation temperature (at 600 °C) can create several holes on the basal plane of the mrGO-600.[30, 36, 37] Such point defects make the mrGO-600 structure difficult to understand in terms of chemical environments when single characterization tools, such as XPS, are employed.[30-32] As a result, these point defects in graphitic carbon regions make the isolated and disconnected sp^2 carbon area in the mrGO-600 surface.

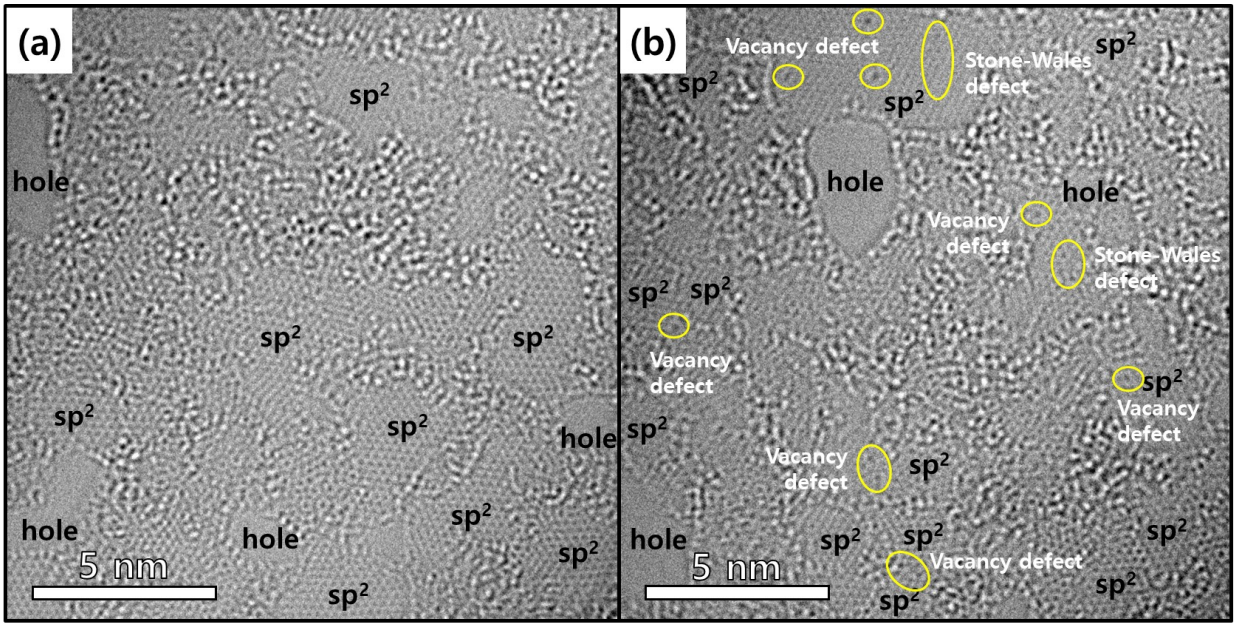

Figure 3. HR-TEM images of mrGO (a) and mrGO-600 (b). The thermal treatment is increased sp^2 carbon domain size from at 14% for the mrGO surface to at 22 % for the mrGO-600 surface.

Peroxide formation activity and active site are determined from I) electrospectroscopy (Figure 4) of both mrGO and mrGO-600 catalysts acquired using a modified H-cell in O_2-saturated 0.1M KOH electrolyte without stirring to characterize IR spectra. Both catalysts show strong and broad peaks ranging from 3000 to 3600 cm^{-1}, which is likely related to the generated peroxide or adsorbed carboxylic acid .[27,28,38] These in-situ IR data indicate that both catalysts can

generate peroxide during the ORR, which is similar to the previous studies.[6,25] More interestingly, we can observe asymmetric carbonate vibration at 1650 and 1550 cm^{-1} due to interactions between the catalytic active site and adsorbed reaction intermediates.[39] This means that O_2 molecules are chemically adsorbed on certain sp^2 carbons during the ORR. Of note, no chemical structural changes are observed before and after ORR measured at 0.6 V vs. RHE in pH 1 electrolyte (**Figure S7**). Based on the in-situ IR spectroelectrochemistry along with the previous studies,[6,25] we therefore conclude that the sp^2 carbon at the grain boundary between ether group and non-continuous graphitic area can convert to peroxide effectively from oxygen molecules like un-annealed mrGO surface.

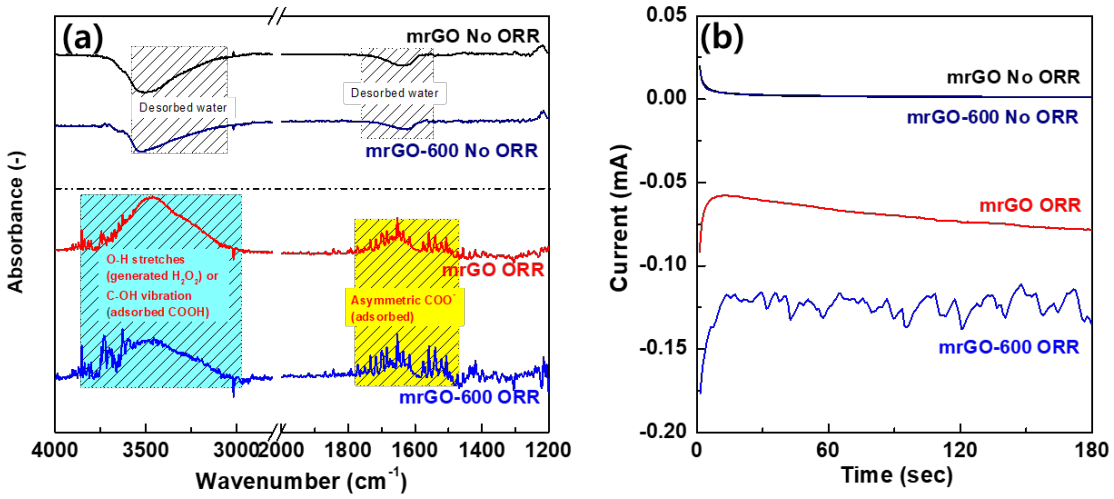

Figure 4. In-situ IR spectroelectrochemistry of both catalysts (b) and current responses during the in-situ measurements applied constant potential at 1.1 V (for No ORR) and 0.8 V (for ORR) vs. RHE in O_2-saturated 0.1M KOH without stirring (b).

CONCLUSIONS

In conclusion, we attempted to describe the detailed chemical and morphological structure of the mrGO-600 using various analytic techniques such as XPS, Raman, IR, NAEXFS, and HR-TEM. We also attempted to understand high peroxide formation activity of the mrGO-600 surface in terms of chemical groups and structural morphology. The extensive characterizations suggest that the mrGO-600 structure consists of disconnected sp^2 carbon region that contains various point defects in the graphitic area, along with amorphous carbon bonding that includes oxygen functional groups, particularly ring ethers. Furthermore, in-situ IR electrospectroscopy can take a snapshot that interacts between the catalytic active sites and the peroxide-generated intermediates, which provides a strong evidence that sp^2 carbons is active sites for electrocatalytic peroxide generation. Because of the relatively small size of the sp^2 carbon bonding along with the ring ether groups, the mrGO-600 can selectively promote peroxide formation activity in the alkaline condition. We believe this study can serve as reference for the synthesis of peroxide-selective carbon electrodes and can motivate the characterization of carbon materials in detail including chemical and environmental structures.

EXPERIMENTAL SECTION

Materials We purchased a fine grade synthetic graphite powder (SP-1) from Bay Carbon Inc. (Bay city, MI, USA) and used as received. Daejung Chemicals & Metals Co. (Siheung, Korea) supplied sulphuric acid (H_2SO_4, 97%), hydrochloric acid (HCl, 35% in water), acetone (CH_3COCH_3, 99.5%). Aldrich Chemical Co. (Milwaukee, WI, USA) provided hydrogen peroxide (H_2O_2, 50% in water), phosphorous pentoxide (P_2O_5, 98%), and

ethylenediaminetetraacetic acid (EDTA, ACS reagent). Potassium permanganate ($KMnO_4$) from JUNSEI Chemical Co. (Tokyo, Japan) were also used as received.

Synthesis of mrGO and mrGO-600 catalysts and preparation of catalyst-coated electrodes The modified Hummers method was used to synthesize GO powder, which describes the previous reports[1]. The mrGO and mrGO-600 preparations were followed by previous protocol. For electrochemical measurements, mrGO catalyst was coated on P50 AvCarb carbon paper (Fuel Cell Store) by a simple dip coating method using dispersed mrGO solution at 0.05 wt.%. The detailed recipe was reported at Ref. 2.

Raman microscopic mapping Raman spectra and mapping were obtained by Raman microscope (LabRam HV Evolution, Horiba, Japan). The mrGO and mrGO-600 films were used for Raman analysis. To prepare the mrGO film, we used a vacuum filtration method. Briefly, 50 mL of a dispersed mrGO solution (at 0.05 wt.% in D.I. water) was poured into the filtration system and then dried the prepared film in vacuum oven at 100 ^oC for overnight. The mrGO-600 film was obtained by thermal treatment by using the prepared mrGO film in tube furnace at 600 ^oC for 3 hours (a ramp rate is 10 ^oC/min) under N_2 purge. A laser beam with 532 nm wavelength was used as the excitation source, and the laser excitation was focused using a x100 objective. Raman mapping images were collected within a 6×6 μm^2–sized area to visualize I_D, I_G, and I_D/I_G bands.

In-situ IR electrospectroscopy The working electrode prepared on Si prism was placed in a one-compartment, three electrode spectroelectrochemical cell. mrGO or mrGO-600 were used for working electrode, Ag/AgCl (Basi, 3M NaCl) for reference electrode, and the platinum wire was used for counter electrode. The cell was integrated into the Fourier Transform Infrared Spectrophotometer (FT-IR, Nicolet IS50, Thermo Fischer Scientific) equipped with a mercury cadmium telluride (MCT) detector and a variable angle specular reflectance accessory (Veemax Ⅲ, Pike technologies). Electrochemical measurements were carried out with an Autolab PGSTAT204 potentiostat. All measurements were carried out in O_2-saturated 0.1 M KOH electrolytes without stirring at room temperature. Constant O_2 flow (at 20 sccm) controlling mass flow controllers (MC-100SCCM-D; Alicat Scientific) was kept into the electrolytes during the measurements. All spectroscopic measurements were conducted at a 4 cm^{-1} spectral resolution

Electrode preparation for in-situ IR measurement Au thin films were prepared by an electrodeless plating procedure.[40] The reflecting plane of a 60° Si prism (Veemax, 2 cm in diameter) was sequentially polished with alumina pastes for 10-15 min each to reveal a fresh Si layer. The crystal was then rinsed in a constant stream of DI water for 5-10 min while rubbing it with a wet Kimwipe. Sequentially, the Si surface was etched by immersing the reflecting plane of the prism in an aqueous solution of 40 wt. % NH_4F (25 °C) for 1 min. After etching, the prism was rinsed with DI water and the reflecting surface was immersed in the mixture of the Au plating solution (0.015 M $NaAuCl_4 \cdot 2H_2O$ + 0.15 M Na_2SO_3 + 0.05 M $Na_2S_2O_3 \cdot 5H_2O$ + 0.05 M NH_4Cl and a 2 wt.% hydrofluoric acid solution in a 1:2 volume ratio; T = 60 °C) for 2 min, rinsed with DI water and dried in air before the spray coating. mrGO and mrGO-600 ink was prepared by mixing 0.3ml of as-prepared dispersed mrGO and mrGO-600 solution and 6 µl of

nafion solution into 0.3 ml of DI and the ink was sonicated for 15 min. Then, 0.5 ml of ink was sprayed on Au electrode with 0.5 cm^2 of active area using spraying gun. The electrode was dried in 80°C oven for more than 30 min and used for the electrochemical reactions.

Material characterization X-ray photoelectron spectroscopy (XPS) was used to equip a monochromatized Al Kα X-ray source (Quantum2000, Physical electronics, Chanhassen, MN, USA). Carbon bonds of the catalysts were characterized from C1s peak data. Deconvolution was performed by Gaussian peak after correcting a Shirley base line to distinguish each peak, which is well-established tool for XPS analysis. Chemical conformation was obtained to use FT-IR (Bruker VERTEX 80v, MA, USA) equipped with a high-resolution detector (Mercury Cadmium Telluride). Mixture ratio of potassium chloride and each material is 1000 to 1 for preparation of IR pellets. This identical mixture enables to roughly estimate functional group ratio from application of peak intensity of each functional group. NEXAFS experiments on beamline 8.0.1.4 (wet-RIXS endstation) at the Advanced Light Source, Lawrence Berkeley National Laboratory were used. Previous literatures described the NEXAFS measurements in detail.[2, 3] Calibration of energy scales for the NEXAFS spectra was employed a TiO_2 standard, and then normalized to the absorption pre- and post-edges. Resolution for each spectra was 0.2 eV. A Horiba Jobin-Yvon LabRAM HR800 μ–Raman with 532 nm excitation from a 250 mW diode laser was used to obtain Raman spectra.

ASSOCIATED CONTENT

Supporting Information. Figures S1-S7. This material is available free of charge via the Internet at http://pubs.acs.org.

AUTHOR INFORMATION

Corresponding Authors

*E-mails: wkim@sookmyoung.ac.kr (W. Kim) and khw0605@kangwon.ac.kr (H.W. Kim)

Author Contributions

†T.H. Lee, S. Park, and T.H. Choi equally contributed to this work. All authors have given approval to the final version of the manuscript.

Notes

The authors declare no competing financial interest.

ACKNOWLEDGMENT

H.W.K. gratefully acknowledges support from the Technology Innovation Program (20010768) funded by the Ministry of Trade, Industry & Energy (MOTIE, Korea). J.K. acknowledges financial support from a National Research Foundation of Korea grant funded by the Korean Government (2019M2EA1064109). HBP and THL acknowledge support by a Korea Research

Institute of Chemical Technology (KRICT) grant funded by the Korean government (Ministry of Science and ICT) in 2019 (CRC-14-1-KRICT). This research used re-sources of the Advanced Light Source, a U.S. DOE Office of Science User Facility under contract no. DE-AC02-05CH11231.

REFERENCES

1. Seh, Z. W.; Kibsgaard, J.; Dickens, C. F.; Chorkendorff, I. B.; Norskov, J. K.; Jaramillo, T. F. Combining Theory and Experiment in Electrocatalysis: Insights into Materials Design. *Science* **2017,** *355* (146).
2. Campos-Martin, J. M.; Blanco-Brieva, G.; Fierro, J. L. G. Hydrogen Peroxide Synthesis: an Outlook beyond the Anthraquinone Process. *Angew. Chem. Int. Ed.* **2006,** *45* (42), 6962-6984.
3. Jiang, Y.; Ni, P.; Chen, C.; Lu, Y.; Yang, P.; Kong, B.; Fisher, A.; Wang, X. Selective Electrochemical H_2O_2 Production through Two-Electron Oxygen Electrochemistry. *Adv. Energy Mater.* **2018**, 1801909.
4. Zheng, Z.; Ng, Y. H.; Wang, D. W.; Amal, R. Epitaxial Growth of Au-Pt-Ni Nanorods for Direct High Selectivity H_2O_2 Production. *Adv. Mater.* **2016,** *28* (45), 9949-9955.
5. Lu, Z.; Chen, G.; Siahrostami, S.; Chen, Z.; Liu, K.; Xie, J.; Liao, L.; Wu, T.; Lin, D.; Liu, Y.; Jaramillo, T. F.; Nørskov, J. K.; Cui, Y. High-efficiency Oxygen Reduction to Hydrogen Peroxide Catalysed by Oxidized Carbon Materials. *Nat. Catal.* **2018,** *1*, 156-162.
6. Kim, H. W.; Ross, M. B.; Kornienko, N.; Zhang, L.; Guo, J.; Yang, P.; McCloskey, B. D. Efficient Hydrogen Peroxide Generation Using Reduced Graphene Oxide-based Oxygen Reduction Electrocatalysts. *Nat. Catal.* **2018,** *1*, 282-290.
7. Hage, R.; Lienke, A., Applications of Transition-metal Catalysts to Textile and Wood-pulp Bleaching. *Angew. Chem. Int. Ed.* **2006,** *45* (2), 206-222.
8. Lee, H.; Dellatore, S. M.; Miller, W. M.; Messersmith, P. B. Mussel-inspired Surface Chemistry for Multifunctional Coatings. *Science* **2007,** *318* (5849), 426-430.
9. Yang, H. H.; McCreery, R. L. Elucidation of the Mechanism of Dioxygen Reduction on Metal-free Carbon Electrodes. *J. Electrochem. Soc.* **2000,** *147* (9), 3420-3428.
10. Yeager, E. Electrocatalysts for O_2 reduction. *Electrochim. Acta* **1984,** *29* (11), 1527-1537.
11. Chen, S.; Chen, Z.; Siahrostami, S.; Kim, T. R.; Nordlund, D.; Sokaras, D.; Nowak, S.; To, J. W.; Higgins, D.; Sinclair, R. Defective Carbon-based Materials for the Electrochemical Synthesis of Hydrogen Peroxide. *ACS Sustain. Chem. Eng.* **2017,** *6* (1), 311-317.
12. Bukas, V. J.; Kim, H. W.; Sengpiel, R.; Knudsen, K. B.; Voss, J.; McCloskey, B. D.; Luntz, A. C. Combining Experiment and Theory to Unravel the Mechanism of Two-Electron Oxygen Reduction at a Selective and Active Co-Catalyst. *ACS Catal.* **2018,** *8*, 11940-11951.
13. Tan, X.; Tahini, H. A.; Smith, S. C. Understanding the High Activity of Mildly Reduced Graphene Oxide Electrocatalysts in Oxygen Reduction to Hydrogen Peroxide. *Mater. Horiz.* **2019,** *6*, 1409-1415.

14. Li, Z.; Jiang, Y.; Liu, C.; Wang, Z.; Cao, Z.; Yuan, Y.; Li, M.; Wang, Y.; Fang, D.; Guo, Z. Emerging Investigator Series: Dispersed Transition Metals on a Nitrogen-doped Carbon Nanoframework for Environmental Hydrogen Peroxide Detection. *Environ. Sci.: Nano* **2018,** *5* (8), 1834-1843.
15. Mitraka, E.; Gryszel, M.; Vagin, M.; Jafari, M. J.; Singh, A.; Warczak, M.; Mitrakas, M.; Berggren, M.; Ederth, T.; Zozoulenko, I. Electrocatalytic Production of Hydrogen Peroxide with Poly (3, 4-ethylenedioxythiophene) Electrodes. *Adv. Sustainable Syst.* **2019,** *3* (2), 1800110.
16. Sa, Y. J.; Kim, J. H.; Joo, S. H. Active Edge-Site-Rich Carbon Nanocatalysts with Enhanced Electron Transfer for Efficient Electrochemical Hydrogen Peroxide Production. *Angew. Chem. Int. Ed.* **2019,** *58* (4), 1100-1105.
17. Zhu, J.; Xiao, X.; Zheng, K.; Li, F.; Ma, G.; Yao, H.-C.; Wang, X.; Chen, Y. KOH-treated Reduced Graphene Oxide: 100% Selectivity for H_2O_2 Electroproduction. *Carbon* **2019,** *153*, 6-11.
18. Hu, R.; Yao, F.; Wu, C.; Jin, C.; Guan, L. Enhancing the Production of Hydrogen Peroxide from Electrocatalytic Oxygen Reduction Reaction by Tailoring the Electronic States of Single-walled Carbon Nanotubes: a Synergistic Effect from Interior Filling and Exterior Oxidation. *Sustain. Energ. & Fuels* **2019,** *3*, 1951-1956.
19. Hu, R.; Wu, C.; Hou, K.; Xia, C.; Yang, J.; Guan, L.; Li, Y. Tailoring the Electrocatalytic Oxygen Reduction Reaction Pathway by Tuning the Electronic States of Single-walled Carbon Nanotubes. *Carbon* **2019,** *147*, 35-42.
20. Kim, H. W.; Park, H.; Roh, J. S.; Shin, J. E.; Lee, T. H.; Zhang, L.; Cho, Y. H.; Yoon, H. W.; Bukas, V. J.; Guo, J. Carbon Defect Characterization of Nitrogen-Doped Reduced Graphene Oxide Electrocatalysts for the Two-Electron Oxygen Reduction Reaction. *Chem. Mater.* **2019,** *31* (11), 3967-3973.
21. Lai, L. F.; Potts, J. R.; Zhan, D.; Wang, L.; Poh, C. K.; Tang, C. H.; Gong, H.; Shen, Z. X.; Jianyi, L. Y.; Ruoff, R. S. Exploration of the Active Center Structure of Nitrogen-doped Graphene-based Catalysts for Oxygen Reduction Reaction. *Energ. Environ. Sci.* **2012,** *5* (7), 7936-7942.
22. Higgins, D.; Chen, Z.; Chen, Z. Nitrogen Doped Carbon Nanotubes Synthesized from Aliphatic Diamines for Oxygen Reduction Reaction. *Electrochim. Acta* **2011,** *56* (3), 1570-1575.
23. Li, Q.; Zhang, S.; Dai, L.; Li, L.-s. Nitrogen-doped Colloidal Graphene Quantum Dots and their Size-dependent Electrocatalytic Activity for the Oxygen Reduction Reaction. *J. Am. Chem. Soc.* **2012,** *134* (46), 18932-18935.
24. Parvez, K.; Yang, S.; Hernandez, Y.; Winter, A.; Turchanin, A.; Feng, X.; Müllen, K. Nitrogen-doped Graphene and its Iron-based Composite as Efficient Electrocatalysts for Oxygen Reduction Reaction. *ACS Nano* **2012,** *6* (11), 9541-9550.
25. Kim, H. W.; Bukas, V. J.; Park, H.; Park, S. J.; Diederichsen, K. M.; Lim, J.; Cho, Y. H.; Yoon, H. W.; Kim, W.; Han, T. H. Mechanisms of Two-electron and Four-electron Electrochemical Oxygen Reduction Reactions at Nitrogen-doped Reduced Graphene Oxide. *ACS Catal.* **2019,** *10* (1), 852-863.
26. Dreyer, D. R.; Park, S.; Bielawski, C. W.; Ruoff, R. S. The Chemistry of Graphene Oxide. *Chem. Soc. Rev.* **2010,** *39* (1), 228-240.

27. Acik, M.; Lee, G.; Mattevi, C.; Chhowalla, M.; Cho, K.; Chabal, Y. J. Unusual Infrared-Absorption Mechanism in Thermally Reduced Graphene Oxide. *Nat. Mater.* **2010,** *9* (10), 840-845.
28. Acik, M.; Lee, G.; Mattevi, C.; Pirkle, A.; Wallace, R. M.; Chhowalla, M.; Cho, K.; Chabal, Y. The Role of Oxygen during Thermal Reduction of Graphene Oxide Studied by Infrared Absorption Spectroscopy. *J. Phys. Chem. C* **2011,** *115* (40), 19761-19781.
29. Ferrari, A. C. Raman Spectroscopy of Graphene and Graphite: Disorder, Electron–phonon Coupling, Doping and Nonadiabatic Effects. *Solid State Commun.* **2007,** *143* (1-2), 47-57.
30. Erickson, K.; Erni, R.; Lee, Z.; Alem, N.; Gannett, W.; Zettl, A. Determination of the Local Chemical Structure of Graphene Oxide and Reduced Graphene Oxide. *Adv. Mater.* **2010,** *22* (40), 4467-4472.
31. Gómez-Navarro, C.; Meyer, J. C.; Sundaram, R. S.; Chuvilin, A.; Kurasch, S.; Burghard, M.; Kern, K.; Kaiser, U. Atomic Structure of Reduced Graphene Oxide. *Nano Lett.* **2010,** *10* (4), 1144-1148.
32. Mkhoyan, K. A.; Contryman, A. W.; Silcox, J.; Stewart, D. A.; Eda, G.; Mattevi, C.; Miller, S.; Chhowalla, M. Atomic and Electronic Structure of Graphene-Oxide. *Nano Lett.* **2009,** *9* (3), 1058-1063.
33. Lee, V.; Dennis, R. V.; Schultz, B. J.; Jaye, C.; Fischer, D. A.; Banerjee, S. Soft X-ray Absorption Spectroscopy Studies of the Electronic Structure Recovery of Graphene Oxide upon Chemical Defunctionalization. *J. Phys. Chem. C* **2012,** *116* (38), 20591-20599.
34. Lee, V.; Dennis, R. V.; Jaye, C.; Wang, X.; Fischer, D. A.; Cartwright, A. N.; Banerjee, S. In situ Near-edge Xray Absorption Fine Structure Spectroscopy Investigation of the Thermal Defunctionalization of Graphene Oxide. *J. Vac. Sci. Technol. B* **2012,** *30* (6), 061206.
35. Zhang, L.; Ji, L.; Glans, P.-A.; Zhang, Y.; Zhu, J.; Guo, J. Electronic Structure and Chemical Bonding of a Graphene Oxide–sulfur Nanocomposite for Use in Superior Performance Lithium–sulfur Cells. *Phys. Chem. Chem. Phys.* **2012,** *14* (39), 13670-13675.
36. López, V.; Sundaram, R. S.; Gómez-Navarro, C.; Olea, D.; Burghard, M.; Gómez-Herrero, J.; Zamora, F.; Kern, K. Chemical Vapor Deposition Repair of Graphene Oxide: A Route to Highly-Conductive Graphene Monolayers. *Adv. Mater.* **2009,** *21* (46), 4683-4686.
37. Cheng, M.; Yang, R.; Zhang, L.; Shi, Z.; Yang, W.; Wang, D.; Xie, G.; Shi, D.; Zhang, G. Restoration of Graphene from Graphene oxide by Defect Repair. *Carbon* **2012,** *50* (7), 2581-2587.
38. Pettersson, M.; Tuominen, S.; Räsänen, M. IR Spectroscopic Study of H_2O_2, HDO_2, and D_2O_2 Isolated in Ar, Kr, and Xe Matrices. *J. Phy. Chem. A* **1997**, 101(6), 1166-1171.
39. Denton, J. K.; Kelleher, P. J.; Johnson, B. A.; Baer, M. D.; Kathmann, S. M.; Mundy, C. J.; Rudd, W.; Allen, H. C.; Choi, T. H.; Jordan, K. D. Molecular-Level Origin of the Carboxylate Head Group Response to Divalent Metal Ion Complexation at the Air-Water Interface. *Proc. Natl. Acad. Sci.* **2019**, 116(30), 14874-14880.
40. Miyake, H.; Ye, S. Electroless Deposition of Gold Thin Films on Silicon for Surface-Enhanced Infrared Spectroelectrochemistry. *Electrochem. Commun.* **2002**, 4(12), 973-977.

Table of Contents (ToC) Figure

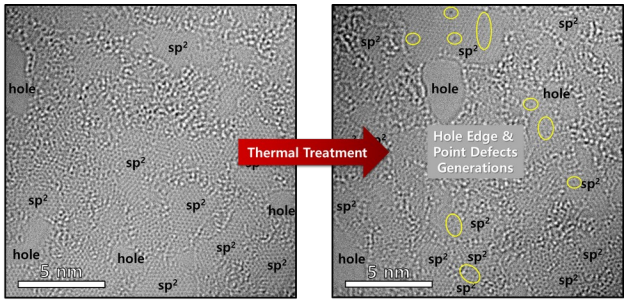
sp²
hole
sp²
sp²
hole
hole
sp²
sp²
5 nm
Thermal Treatment
sp²
sp²
sp²
hole
hole
Hole Edge &
Point Defects
Generations
sp²
sp²
sp²
hole
sp²
sp²
sp²
5 nm
sp²